Bio-Design and Manufacturing (2021) 4:72–86
https://doi.org/10.1007/s42242-020-00107-2

RESEARCH ARTICLE

Bilayer nicorandil-loaded small-diameter vascular grafts improve endothelial cell function via PI3K/AKT/eNOS pathway

Zheng Xing[1] · Chen Zhao[2] · Chunchen Zhang[3,4] · Yubo Fan[1] · Haifeng Liu[1]

Received: 9 September 2020 / Accepted: 24 October 2020 / Published online: 19 November 2020

Abstract

For the surgical treatment of cardiovascular disease (CVD), there is a clear and unmet need in developing small-diameter (diameter < 6 mm) vascular grafts. In our previous work, sulfated silk fibroin (SF) was successfully fabricated as a potential candidate for preparing vascular grafts due to the great cytocompatibility and hemocompatibility. However, vascular graft with single layer is difficult to adapt to the complex internal environment. In this work, polycaprolactone (PCL) and sulfated SF were used to fabricate bilayer vascular graft (BLVG) to mimic the structure of natural blood vessels. To enhance the biological activity of BLVG, nicorandil (NIC), an FDA-approved drug with multi-bioactivity, was loaded in the BLVG to fabricate NIC-loaded BLVG. The morphology, chemical composition and mechanical properties of NIC-loaded BLVG were assessed. The results showed that the bilayer structure of NIC-loaded BLVG endowed the graft with a biphasic drug release behavior. The in vitro studies indicated that NIC-loaded BLVG could significantly increase the proliferation, migration and antioxidation capability of endothelial cells (ECs). Moreover, we found that the potential biological mechanism was the activation of PI3K/AKT/eNOS signaling pathway. Overall, the results effectively demonstrated that NIC-loaded BLVG had a promising in vitro performance as a functional small-diameter vascular graft.

Keywords Bilayer vascular grafts · Nicorandil · Sulfated silk fibroin · Endothelial cell function · PI3K/AKT/eNOS pathway

Introduction

Cardiovascular disease (CVD) is still the primary cause of morbidity and mortality worldwide, and coronary artery disease (CAD) is the most extrusive form of CVD [1, 2]. Occlusion of blood vessels is the main reason of CVD, which impedes blood supply to crucial organs. Coronary artery bypass grafting (CABG) is commonly used in therapeutic strategies of CVD [3]. Surgeons often consider autologous vessels such as saphenous vein as their first choice for CABG. However, donor-site morbidity and autologous vascular deficiency limited the application of autologous grafts [4]. Thus, it is urgent and crucial to develop artificial vascular grafts as an alternative in CABG.

Currently, there are still many confusing problems in the research of artificial vascular grafts, especially in small-diameter vascular grafts (diameter < 6 mm), including difficulty in spontaneous endothelialization and acute thrombosis [5, 6]. These problems are usually related to vascular endothelial cell (EC) functions of the patients. Compared with healthy people, EC functions in CABG patients are significantly reduced, due to the complications such asatherosclerosis, diabetes and other chronic diseases [7, 8]. The endothelial dysfunction directly reduces the long-term patency rate of patients after bypass surgery [9]. Therefore, designing and fabricating novel small-diameter vascular grafts combined with bioactive components to improve EC functions and solve acute thrombosis problems at the same time is a feasible strategy.

✉ Haifeng Liu
haifengliu@buaa.edu.cn

1 Key Laboratory for Biomechanics and Mechanobiology of Ministry of Education, School of Biological Science and Medical Engineering, Beijing Advanced Innovation Centre for Biomedical Engineering, Beihang University, Xue Yuan Road No. 37, Haidian District, Beijing 100191, China

2 School of Pharmaceutical Sciences, Tsinghua University, Beijing 100084, China

3 Key Laboratory of Biomedical Engineering of Ministry of Education, Zhejiang University, Hangzhou 310027, China

4 Zhejiang Provincial Key Laboratory of Cardio-Cerebral Vascular Detection Technology and Medicinal Effectiveness Appraisal, Zhejiang University, Hangzhou 310027, China

Nicorandil (N-(2-hydroxyethyl)-nicotinamide nitrate) (NIC), a adenosine triphosphate (ATP)-sensitive potassium (KATP) channel opener combined with nitric oxide (NO) donor activity and antioxidant activity, is clinically used as an antianginal drug [10]. However, many researchers believed that NIC could contribute beneficial effects in cardiovascular system. Umaru et al. reported that NIC could promote angiogenesis via improving the migration capability and network functions of ECs [11]. Serizawa et al. proved that NIC could regulate endothelial dysfunction caused by chronic disease through its antioxidative effects [12]. Horinaka et al. showed that NIC could prevent ventricular remodeling and degradation of cardiac function through upregulating cardiac endothelial NO synthase (eNOS) expression by activating K_{ATP} channels [13]. In addition, compared with some novel compounds, as an FDA-approved drug, NIC is more safe for further clinical applications [14]. Therefore, we decided to add NIC in our vascular graft as a bioactive component to enhance EC functions and accelerate spontaneous endothelialization of vascular grafts.

Silk fibroin (SF) is a natural polymer extracted from Bombyx mori cocoons. Due to minimal immunogenicity, controllable biodegradability and suitable mechanical properties, SF-based scaffolds are used as alternatives to the clinically approved artificial grafts [15–17]. In recent years, several studies have shown that SF is an attractive biomaterials for vascular applications withgreat potential for developing small-diameter vascular grafts [18–20]. In our previous study, we fabricated sulfated SF to impart anticoagulant activity on SF. The results showed that both sulfated SF-based biomaterials and sulfated SF coating materials had great anticoagulant activity. In addition, vascular cells attached and proliferated well on the surface of sulfated SF [21–23]. Thus, to solve acute thrombosis problem after bypass surgery as well as improve the hemocompatibility of vascular graft, using sulfated SF as the substrate of vascular graft is a reasonable and attractive choice.

However, application of single-layer vascular graft is hard to receive satisfactory results in clinical application. Thus, designing multilayer biomimetic structure vascular graft will be an effective way in future studies [24, 25]. As a facile, versatile and cost-effective technology, electrospinning has been widely used in developing multilayer scaffolds [26, 27]. In recent years, many researchers have used electrospinning to develop multilayer vascular graft [28, 29]. Moreover, the micro-/nanofibers fabricated by electrospinning can become a great drug delivery system, and their drug release behavior can be manipulated by regulating fiber diameter and porosity [30, 31]. Yang et al. combined decellularized rat aorta (DRA) and electrospun PCL to fabricate a hybrid vascular graft, loading rapamycin (RM) in the PCL layer. The results of in vitro release study showed that the vascular graft exhibited controlled and sustained release of RM [32]. Shi et al. prepared an aspirin-triggered resolvin D1 (AT-RvD1)-loaded electrospun vascular graft that could continuously release AT-RvD1 over 7 days [33]. Therefore, electrospinning technology has great potential in making multilayer vascular grafts with drug delivery capability.

In this study, a bilayer vascular graft loaded with NIC was fabricated with electrospinning technology. Poly(ε-caprolactone) (PCL), a biocompatible polymer approved by FDA, was used to prepare the thick outer layer of vascular graft, mimicking the smooth muscle layer of natural blood vessels [34]. Thin inner layer was fabricated by sulfated SF to mimic the endothelial layer. NIC was utilized as a bioactive component, loaded in both the outer layer and inner layer to achieve biphasic release based on fiber diameter and porosity. We assessed the morphology, chemical composition, wettability and mechanical properties of the nicorandil-loaded bilayer vascular graft (NIC-loaded BLVG). In vitro drug release behavior and its effect on EC function were also detected. Moreover, the molecular mechanism of NIC-loaded BLVG-mediated EC function increase was investigated by western blot assay.

Materials and methods

Chemicals and materials

Poly(ε-caprolactone) (PCL, Mn = 80,000), chlorosulfonic acid, pyridine and collagenase II was obtained from Sigma-Aldrich (St. Louis, Mo., USA). Raw Bombyx mori silk fibers were supplied from Suzhou Maoda Textile Co., Ltd (Suzhou, China). Nicorandil (NIC) were obtained from Dalian meilunbio Co., Ltd (Dalian, China). Endothelial cell medium (ECM) were obtained from Sciencell (San Diego, CA., USA). Sodium carbonate anhydrous (Na_2CO_3), hydrogen peroxide (H_2O_2), calcium chloride anhydrous ($CaCl_2$), methanol, ethanol, chloroform ($CHCl_3$) and 1,1,1,3,3,3-hexafluoro-2-propanol (HFIP) were obtained from Aladdin Biochemical Technology Co., Ltd. (Shanghai, China). 0.25% trypsin, 4′,6′-diamidino-2-phenylindole hydrochloride (DAPI) solution, TRITC phalloidin, 4% paraformaldehyde (PFA), Triton X-100, phosphate buffer saline (PBS, pH = 7.4), mounting medium, glass coverslips, dimethyl sulfoxide (DMSO), RIPA buffer, CCK-8 assay kit, BCA kit, SDS-PAGE gel kit, SDS-PAGE electrode buffer, WB transfer buffer, nonfat powdered milk, Tris-buffered saline, Tween 20, polyvinylidene fluoride (PVDF) membrane and ECL western blotting substrate were obtained from Solarbio lifescience (Beijing, China). Primary antibody against Akt (ab179463), p-Akt (ab38449), p-PI3K (ab182651) and p-eNOS (ab230158) was obtained from Abcam (Cambridge, UK). Primary antibody against PI3K (#4292), eNOS (#32027) and β-actin (#3700) was obtained from Cell Signaling Technology (Boston,

MA., USA). Secondary antibody ZB-2301 and ZB-2305 was obtained from Beijing ZSGB-BIO Co., Ltd (Beijing, China). Ultrapure water was produced with a Millipore Milli-Q Reference ultrapure water purifier (Molsheim, France). All materials, unless stated, were of analytical grade.

Preparation of sulfated silk fibroin

SF solution was fabricated according to a previously published procedure [35]. First, the raw silk fibers were degummed in 0.1% (w/v) sodium carbonate anhydrous solution at 100 °C for over 30 min. Then, the degummed silk fibers were rinsed in ultrapure water three times to ensure the remnant sericin had been removed. Degummed silk fibers were next dissolved in a mix solution which formed by calcium chloride anhydrous, ethanol and ultrapure water (mole ratio = 1:2:8) at 80 °C with continuous stirring. After the degummed silk fibers were completely dissolved, the SF solution was dialyzed against ultrapure water using a Snake-Skin Pleated Dialysis Tubing (PIERCE, MWCO 3500) at room temperature for over 3 days, and the ultrapure water in dialysis container was changed every 6 h. Finally, the SF solution was freeze-dried for 48 h to prepare SF sponges and kept in a vacuum-drying desiccator for future use.

Sulfated SF was fabricated according to our previously study [21]. Chlorosulfonic acid (10 mL) was slowly added into pyridine (60 mL) in an ice bath and put SF sponges (1 g) into the mixture solution. Then, continuously stirred the reaction system, which was in a thermostatically controlled bath (temperature gradually increased from 0 to 80 °C). After reaction for 1 h, about 200 mL ultrapure water was added into the reaction system and the system was subsequently neutralized by equivalent molar sodium hydroxide solution. Vacuum filtration was used to remove insoluble materials before the remaining soluble portion was precipitated by adding ethanol (500 mL). The precipitate was harvested by centrifuging (4 °C, 10,000 rpm for 20 min), then the supernatant was discarded and the precipitate was redissolved with small amount of ultrapure water. Sulfated SF solution was followed by dialyzed and freeze-drying, and the procedure was same as the SF solution.

Fabrication of NIC-loaded BLVG

NIC-loaded BLVG was fabricated by electrospinning using an apparatus as shown in Fig. 1a. The device included a single nozzle system, syringe pump (KD Scientific, KDS100, USA), high-power voltage supply (Glassman high voltage Inc. series FC, USA), a rotatable collector and a jet imaging device (CCD camera) (Baumer TXG02C, Germany). Briefly, formulated liquid was injected into capillaries with 21G stainless steel needle which was controlled by precision syringe pumps. For all NIC-loaded BLVG, formulated media for outer layer consisted of 18 w/v% PCL are dissolved in methanol/$CHCl_3$/ (1:5, v/v) mix solution and 0.9 w/v% NIC powder was dispersed in the solution. The inner layer consisted of 12 w/v% sulfated SF dissolved in HFIP and 0.6 w/v% NIC powder dispersed in the liquid. The flow rates of outer-layer and inner-layer formulations were fixed at 8 and 2 mL/h. And the electric field condition was 14 kV for both inner and outer layers prepared. The collection distance between nozzle and collector was 17 cm and 15 cm, respectively. The diameter of the stainless steel mandrel on the rotatable collector was 2 mm, and the rotation speed of the device was 300 rpm/min. To fabricate NIC-loaded BLVG, the inner layer electrospinning parameters were used as step 1, followed by outer layer parameters as step 2. After these two steps, the graft was removed from the stainless steel mandrel and placed into a vacuum dryer for over 48 h to remove the residual solvent. Before using NIC-loaded BLVG for further research, the graft was exposed to UV light for over 48 h as sterilization. All grafts were fabricated at room temperature (25 °C).

Characterization of NIC-loaded BLVG

Morphology study

The morphology and structure of the electrospun grafts were examined using a scanning electron microscopy (SEM, FEI QUANTA FEG250, USA). All samples were sputtering coated with platinum for 90 s and observed at an acceleration of 10 kV. Based on the SEM images, the average fiber diameter and pore size of each sample were analyzed with ImageJ software (NIH). At least 100 fibers and 70 pores were manually analyzed in this part. The porosity of different samples were detected with a liquid intrusion method [36]. Dry samples were weighed and then immersed in liquid overnight for complete wetting. The samples were then gently wiped to remove excess liquid and weighed again. Sample porosity was calculated using the following equations:

$$V_{\text{liquid}} = \frac{M_{\text{wet}} - M_{\text{dry}}}{Q_{\text{liquid}}},$$

$$V_{\text{sample}} = \frac{M_{\text{dry}}}{Q_{\text{sample}}},$$

$$\text{Porosity} = \frac{V_{\text{liquid}}}{\left(V_{\text{liquid}} + V_{\text{sample}}\right)} \times 100\%.$$

Here, M_{dry} represented the dry weights of samples. M_{wet} represented the wet weights of samples. Q represented the density.

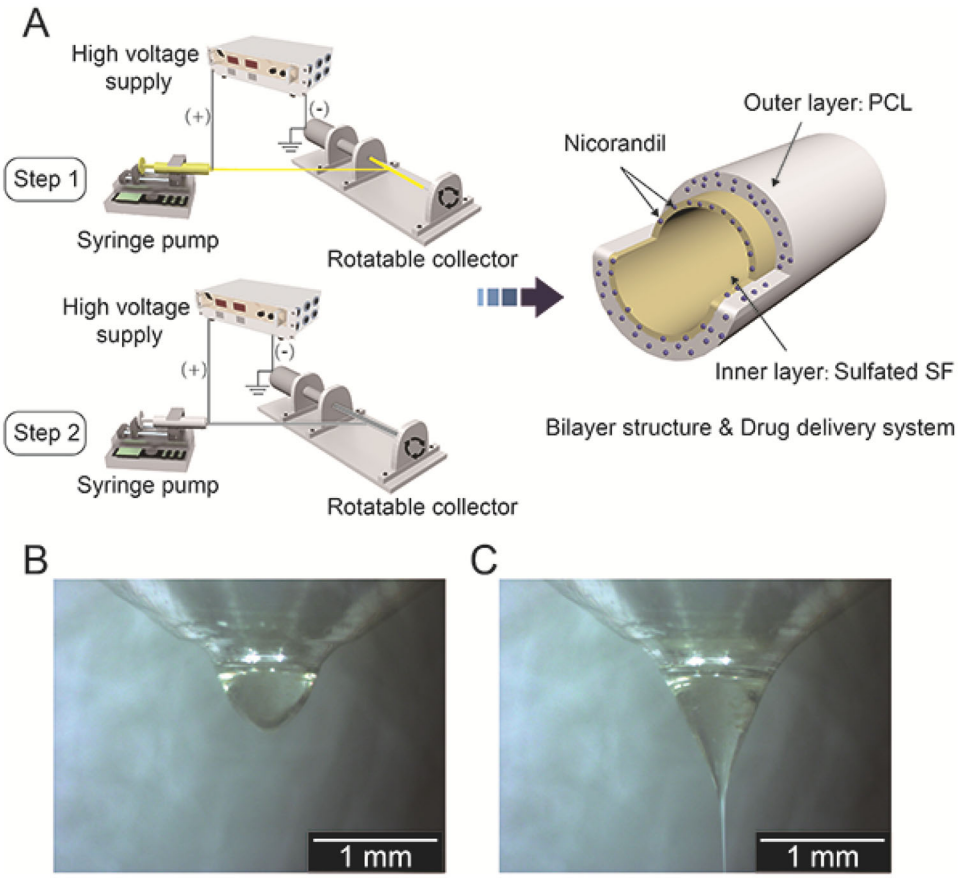

Fig. 1 **a** Schematic diagram of preparing NIC-loaded BLVG by using two-step electrospinning. **b** Digital image of dripping mode of electrospinning process at 0 kV. **c** Digital image of stable jet mode of electrospinning process at 14 kV

Fourier transformed infrared (FTIR) test

In this part, samples were first cut into small pieces, and then, FTIR 7600 spectrophotometer (Lambda Scientific, Australia) was used to analyze the composition and chemical structure. For each measurement, the spectra was recorded in the range of 500–4500 cm^{-1}. Spectra were obtained using 30 scans at a resolution of 4 cm^{-1}.

Wettability

In order to detect wettability of the graft, water contact angle measurements were obtained with a contact angle analyzer (Shanghai Powereach Digital Technology Equipment Co. Ltd., China). A 1 μL droplet of ultrapure water was dropped on the surface of samples. The contact angles were analyzed at the initial state and at 0, 10, 20, 30, 40, 50 and 60 s. Each sample was testedat least 5 times. The mean of the analysis results was used for plotting.

Mechanical test

The mechanical properties of the graft were detected using a universal tester (Instron 3344; Instron, Co. Ltd., UK) with a 100 N load cell at room temperature. Rectangular samples with dimension of 3 × 15 mm and thickness of about 450 μm were used in this test. The distance between two clamps was 2 mm, and the tensile speed was 2 mm/min. The stress–strain curves and other crucial parameters were determined.

NIC loading and in vitro drug release study

The loading capacity (LC) and encapsulation efficiency (EE) of NIC in the graft were measured using the following equations [37, 38]. The LC of NIC in the graft was calculated using Eq. (1):

$$\mathrm{LC}\,(\%) = \frac{\text{Amout of NIC content entarapped in BLVG}\,(\mathrm{mg})}{\text{Weight of BLVG}} \times 100\%. \quad (1)$$

The EE of NIC in the graft was calculated using Eq. (2):

$$\mathrm{EE}\,(\%) = \frac{\text{Amount of NIC content entarapped in BLVG}\,(\mathrm{mg})}{\text{Theoretical total amout of NIC}\,(\mathrm{mg})} \times 100\%. \quad (2)$$

To evaluate NIC release from the graft in vitro, a sample of 200 mg total mass was incubated in 20 mL of PBS buffer. The release of NIC was measured in triplicate under sink conditions at 37 °C. At predetermined time intervals, 2 mL of release solution was transferred for UV–Vis absorption measurements at 262 nm (UV-2600 spectrophotometer, Shimadzu, Japan) [39]. Release medium was replaced with same volume of fresh PBS buffer. The percentage of NIC released was calculated using Eq. (3):

$$\text{NIC release}\ (\%) = \frac{Q_t}{Q_s} \times 100\%. \tag{3}$$

Here, Q_t represented the quantity of NIC released at time t, and Q_s represented the total quantity released.

In vitro cell studies

Cell culture

Human umbilical vein endothelial cells (HUVECs) were extracted from human umbilical cord veins which harvested from Haidian Maternal and Child Health Hospital (Beijing, China). All the procedure was proved by the ethics committee of the hospital. And informed consent was provided according to the Declaration of Helsinki. The endothelial cells (ECs) were detached from the lumen of umbilical vein by trypsinization with 1 mg/mL of collagenase II at 37 °C for 15 min. The detached cells were resuspended and seeded on 10 cm culture dishes and cultured in ECM. The cells were maintained at 37 °C in a humidified incubator with 5% CO_2, and culture medium was changed every 2 days. All the cell harvest procedures were based on our previous studies [40].

Cell proliferation assay

The cells were seed on the bottom of 24-well plates with sterile glass coverslips. Cells were adhered for 24 h. The PCL-VG, BLVG and NIC-loaded BLVG were cut into circular disks with diameter of 13 mm and put into the bottom of 24-well plates. The glass coverslips which seeded with cells were used to cover the samples to avoid sample floating. At predetermined incubation time, cells were removed from incubator and then fixed in 4% PFA for 10 min. Then, the cells were incubated in 0.1% Triton X-100 for 15 min to permeabilize cell membranes. Finally, the cells were stained with TRITC phalloidin and DAPI working solution for 30 min, respectively, to show cytoskeleton and nucleus. The fluorescent signal was detected using confocal microscope (Leica Microsystems GmbH, Mannheim, Germany). This method was based on previous studies [41].

Cell viability

The PCL-VG, BLVG and NIC-loaded BLVG were cut into circular disks with diameter of 10 mm before being placed on the bottom of 48-well plates, and the samples were covered by using sterile glass coverslips to avoid sample floating. ECs were seeded at a density of 5×10^3/well in 300 μL of media. After 6 and 12 h, cell viability was measured by CCK-8 assay. In detail, supernatant was removed and 300 μL of CCK-8 working solution was added in each well to be cultured in 37 °C for another 2 h. Finally, 100 μL of the supernatant was taken and added to 96-well plates. The absorbance at wavelength 450 nm was detected using a micro-plate reader (VersaMax, Molecular Devices, USA). All samples were measured in triplicate.

Cell migration assay

EC migration was studied by wound healing assay. The cells were seeded on the bottom of 24-well plates with sterile glass coverslips. While the cell covers about 80%–90% area of the plate, the PCL-VG, BLVG and NIC-loaded BLVG were cut into circular disks with diameter of 13 mm and put into the bottom of 24-well plates. The wound was uniformed by using 200 μL pipette tip. At predetermined incubation time, cells were stained with TRITC phalloidin and DAPI, the staining procedure is the same as "Cell proliferation assay" section. The cells were observed by using confocal microscope. The migration distance was quantified by using Eq. (4):

$$\text{Migration distance}\ (\%) = \frac{A_0 - A_1}{A_0} \times 100\%. \tag{4}$$

Here, A_0 represented the distance of initial wound distance, A_1 represented the residual distance of wound.

Cell H_2O_2 injury model

ECs were seeded into 24-well plates with sterile glass coverslips. After cells were adhered for 24 h, the supernatant was removed and serum-free medium with 500 μmol/L H_2O_2 was added into each well and incubated for 6 h. The cells were then rinsed three times with PBS to remove residual H_2O_2. Then the PCL-VG, BLVG and NIC-loaded BLVG were cut into circular disks with diameter of 13 mm and put into the bottom of 24-well plates, and the glass coverslips which seeded with cells were used to cover the samples to avoid sample floating. Cells were incubated with the sample for 1 or 2 days. After that, the cells were stained with TRITC phalloidin and DAPI, and the staining and observing procedure was the same as "Cell proliferation assay" section. The cell density was quantified by ImageJ software.

Western blot

Total protein from ECs was harvested in RIPA buffer, and concentration was quantified using BCA assay. Before loading samples in the gels, protein level of ECs was adjusted equally by loading buffer. Then samples of equal volume were loaded in each well. Protein was separated by 10%–12% SDS-PAGE and subsequently transferred to a 0.45 μm PVDF membrane followed by subsequently incubated with 5% non-fat milk in TBST buffer (Tris-buffered saline with 0.1% Tween 20) for 1 h at room temperature. Then, the membranes were incubated with corresponding primary antibody at 4 °C for over 12 h, followed by incubated with secondary antibody at room temperature for 1 h. The membranes were washed 3 times by TBST buffer between each procedure. Immunoreactivity were visualized with an enhanced ECL. The results were analyzed with ImageJ software. The procedure of western blot based on the previous study [42].

Statistical analysis

All the data in this study were presented as mean ± standard error of mean (SEM). Data between two groups were measured with an independent *t*-test, and more than two groups were tested by one-way ANOVA, followed by Tukey's HSD post hoc comparison. Statistical analysis was carried out using SPSS software (SPSS Statistics version 21, IBM, UK). Statistical significance was considered at P values < 0.05. All experiments were performed independently and repeated at least three times.

Results and discussion

Fabrication of NIC-loaded BLVG

NIC-loaded BLVG were successfully fabricated by using electrospinning technology. The schematic diagram of the prepare procedure is shown in Fig. 1a. In detail, the inner layer preparation conditions were firstly used to prepare the thin sulfated SF layer of NIC-loaded BLVG for the growth and proliferation of ECs to mimic the natural endothelial layer. And then, the outer layer preparation conditions were used to prepare the thick PCL layer of NIC-loaded BLVG for the growth and proliferation of SMCs to mimic the natural smooth muscle layer. Figure 1b shows solution yielding the dripping mode once added into nozzle assembly at 0 kV. Under gravitational force, the solution dropped naturally with the infusion of the syringe pump. In contrast, stable jetting behavior of solution was observed at 14 kV (as shown in Fig. 1c). The result suggested the electrospinning process in this study was stable and controllable.

Characterization of NIC-loaded BLVG

The surface morphology of vascular grafts was observed using digital camera and SEM. Figure 2a shows the optical image of NIC-loaded BLVG prepared by electrospinning. SEM images in Fig. 2b showed the clear bilayer structure of NIC-loaded BLVG. Figure 2c shows a partially enlarged image. The bilayer structure consisted of a thin inner layer and a thick outer layer, and the two layers are tightly connected with minimized gap. Figure 2d–g shows the outer layer and inner layer fiber structure of the vascular graft with or without loaded NIC. The presence of NIC did not influence their electrospinnability. And there were no large NIC crystals presenting on the surface of the NIC-loaded fiber group, implying that NIC was homogeneously dispersed in the electrospun fibers. Figure 2h–m shows the statistical histogram of fiber diameters, pore sizes and porosity. The diameters of PCL fibers in outer layer with or without loaded NIC were 7.38 ± 0.17 μm and 7.09 ± 0.27 μm, the pore size was 31.9 ± 1.9 μm and 32.6 ± 1.6 μm, and the porosity was 75.7 ± 3.7% and 76.2 ± 3.0%, respectively. The diameters of sulfated SF fibers in inner layer with or without loaded NIC were 3.11 ± 0.14 μm and 3.02 ± 0.15 μm, the pore size was 6.83 ± 0.4 μm and 6.51 ± 0.27 μm, and the porosity was 45.7 ± 2.3% and 44.6 ± 1.3%, respectively. All the electrospinning fibers had a smooth surface, uniform diameter and pore size. After adding NIC in the electrospinning solution, the diameter of NIC-loaded fiber was slightly increased, but it is not statistically significant.

FTIR spectroscopy was used to confirm the chemical composition of different samples. Figure 3a shows the FTIR curve of SF and sulfated SF. Compared with SF sample, significant changes could be found in the FTIR image of sulfated SF sample. Strong absorptions were shown at 1014.1 and 1058.7 cm^{-1}, which were attributed to the vibrations of organic sulfate salts. Sulfation of SF also caused the progressive increase in intensity and broadening of the bands in the 1180–1300 cm^{-1} range, which was attributed to –S=O stretching vibrations. In both SF and sulfated SF groups, the strong absorptions were shown at 1600 to 1700 cm^{-1} interval, 1520 cm^{-1} and 1540 cm^{-1}, which were attributed to the amide I and II bands of SF. In addition, these characteristic bands in the sulfated SF group shifted a little to high wave numbers, which might be due to the sulfation of SF [21]. This result indicated that the reaction with chlorosulfonic acid succeeded to incorporate sulfate groups in SF molecules. Figure 3b shows the FTIR results of different layers of the vascular grafts. Outer layer was prepared by PCL, and the characteristic absorption peaks of PCL were observed at 2937 cm^{-1}, owing to the asymmetric stretching vibration. The peak at 1726 cm^{-1} indicated –C=O stretching vibration, while the peaks at 1236 cm^{-1} and 1292 cm^{-1} were attributed to –C–O stretching vibrations. The inner layer was

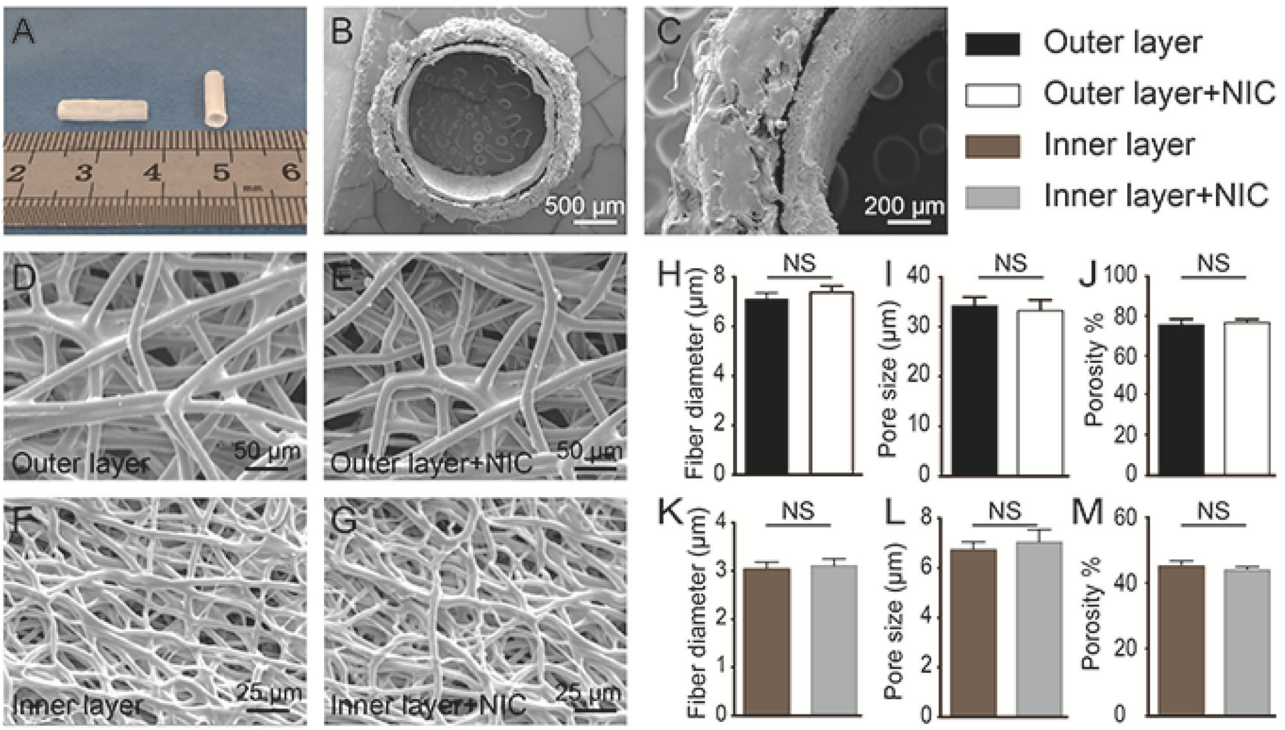

Fig. 2 Morphology of NIC-loaded BLVG. **a** Optical image of NIC-loaded BLVG. **b** SEM image of NIC-loaded BLVG. **c** Local enlargement of bilayer structure vascular graft. **d**, **e** SEM image of outer layer PCL fibers with or without loaded NIC. **f**, **g** SEM image of inner layer sulfated SF fibers with or without loaded NIC. **h**–**m** Statistical results of fiber diameter, pore size and porosity

fabricated by sulfated SF, which was similar as the curve in Fig. 3a. The spectra of NIC showed peaks at 3075 cm^{-1} and 3243 cm^{-1}, owing to aromatic –C–H stretching vibration and amide –N–H stretching vibration. The peaks at 1361 cm^{-1} $–NO_2$ stretching, 1590 cm^{-1} C=C aromatic and 1555 cm^{-1} –N–O asymmetric stretching were also the characteristic peaks of NIC. The characteristic peaks of NIC were not clearly observed at the FTIR spectra of outer layer +NIC group and inner layer +NIC group. This might be due to the relatively low NIC content loaded in the vascular graft in comparison with the main ingredient constituents, and the NIC characteristic peaks were covered by the peak of other constituents. The FTIR spectra of other constituents were not influenced by NIC, indicating that NIC had no chemical interaction between PCL and sulfated SF.

Hydrophilic/hydrophobic characteristics of the different layer of BLVG were detected by water contact angle. In detail, the contact angles of outer layer, outer layer + NIC, inner layer and inner layer +NIC were 105.3 ± 5.7, 100.5 ± 4.5, 65.0 ± 1.4 and 62.5 ± 1.8, respectively. Compared with inner layer, the outer layer had a more hydrophobic surface. The contact angles of these groups were also detected at predetermined time intervals (as shown in Fig. 4). The result indicated that the presence of NIC increased the wettability of both the outer and inner layers. Thus, NIC-

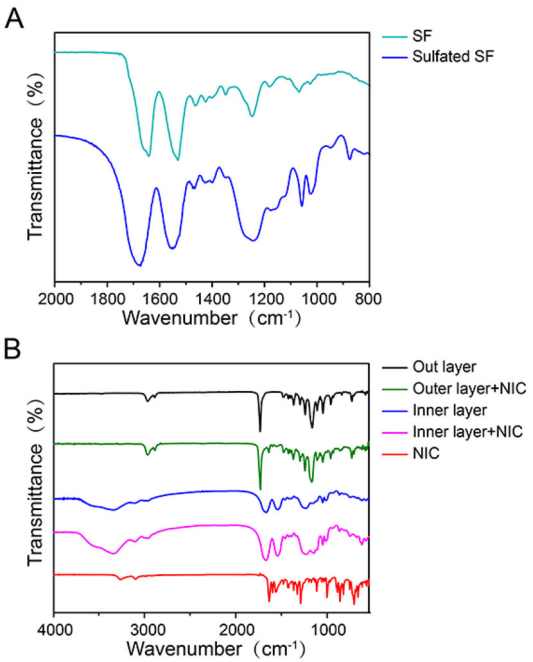

Fig. 3 FTIR spectra. **a** FTIR spectra of SF and sulfated SF. **b** FTIR spectra of different parts of vascular grafts

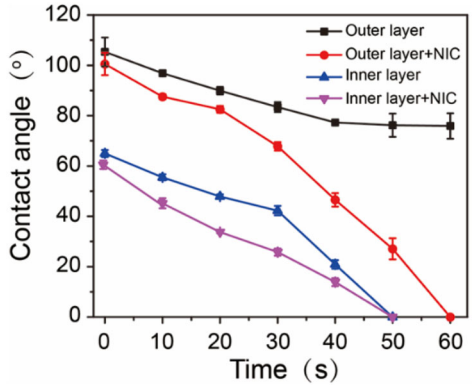

Fig. 4 Water contact angle values of the inner layer and outer layer of BLVG with or without loaded NIC at different times

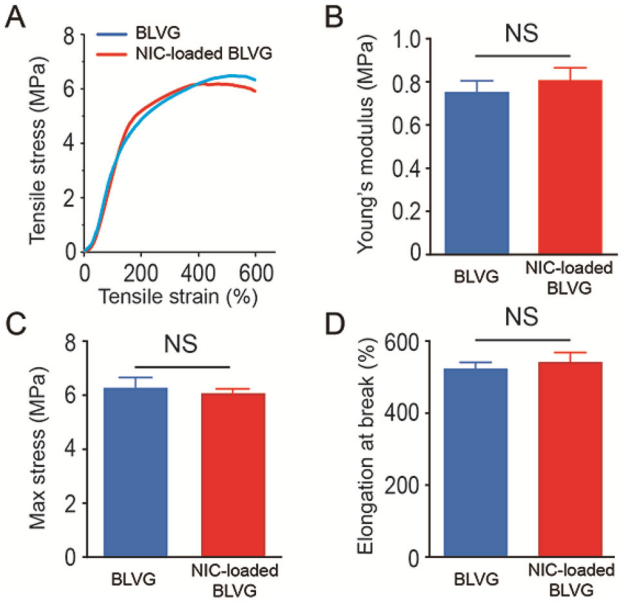

Fig. 5 Mechanical properties. **a** Typical stress–strain curves of BLVG and NIC-loaded BLVG. **b–d** Comparison of the Young's moduli (**b**), max strength (**c**) and elongation at breakage (**d**)

loaded BLVG was more suitable for cell adhesion and growth due to the better wettability compared with the BLVG [43, 44].

The mechanical properties of vascular grafts are crucial for maintaining their shape and structural integrity during surgical procedures. Figure 5a shows the stress–strain curves of BLVG and NIC-loaded BLVG. Figure 5b–d shows the crucial parameter of the graft. In detail, the Young's modulus of BLVG and NIC-loaded BLVG was 0.75 ± 0.06 MPa and 0.81 ± 0.05 MPa, respectively. The max stress was 6.23 ± 0.43 MPa and 6.01 ± 0.23 MPa, respectively. And elongation at break was $522.8 \pm 18.5\%$ and $544.0 \pm 24.2\%$, respectively. These results were similar to those of the vascular grafts prepared by PCL, suggesting that the mechanical strength of BLVG was mainly provided by the outer layer, and loading NIC in the BLVG did not significantly affect the mechanical properties of the graft [45]. All these parameters were higher than those of the natural blood vessels, which suggested that NIC-loaded BLVG was suitable for clinical application including withstanding the force required for bypass suture and maintaining the original lumen structure for blood flow [46].

In vitro release study

Outer layer-loaded BLVG (hosting NIC only in the outer layer of BLVG), inner layer-loaded BLVG (hosting NIC only in the inner layer of BLVG) and NIC-loaded BLVG (NIC loading into both the outer layer and the inner layer of BLVG) were used to detect in vitro drug release behavior based on structural variations. Electrospinning technology was an effective method to load bioactive components into vascular graft in a single step. LC confirmed the feasibility of NIC encapsulation into BLVG, while EE provided an indication on NIC encapsulation levels within BLVG. LCs of outer layer-loaded BLVG, inner layer-loaded BLVG and NIC-loaded BLVG were $4.30 \pm 0.23\%$, $4.61 \pm 0.16\%$, $4.36 \pm 0.18\%$, while the EEs were $85.9 \pm 4.7\%$, $92.3 \pm 3.2\%$, $87.3 \pm 3.6\%$. In vitro release curve of 48 h test period is shown in Fig. 6a (different BLVG schematics shown as insets). The results indicated that BLVG prepared through electrospinning technology successfully loaded NIC into BLVG, which in turn showed the appreciable drug stability during preparing process and high quantities of NIC encapsulation.

The relatively thicker fibers and larger pore sizes of outer layer-loaded BLVG significantly increased the contact area between drug and release medium. Thus, after 24 h, 97.5% of NIC from outer layer-loaded BLVG was released. The inner layer-loaded BLVG with thinner fibers and smaller pore sizes, which hosted NIC only in the inner layer, exhibited sustained release over 96 h (93.1% of contained drug). The results showed that NIC-loaded BLVG displayed a biphasic release pattern, including a burst release period during the first 24 h (72.6% of contained drug) and a sustained release phase from 24 to 96 h (94.3% of contained drug). Sustained release was studied for a further 7 days, and the release profiles are shown in Fig. 6b (release between 0 and 4 h shown as insets). Outer layer-loaded BLVG, inner layer-loaded BLVG and NIC-loaded BLVG released 99.4, 98.8 and 99.5% of the encapsulated drug, respectively, over the extended test period.

Burst release from BLVG was facilitated by the outer layer depending on the large pore size and thick fibers. This outer layer structure could be regulated by changing the contents of infused materials and some key parameters during the electrospinning process. Biphasic release profile from NIC-loaded BLVG indicated that the drug delivery system was

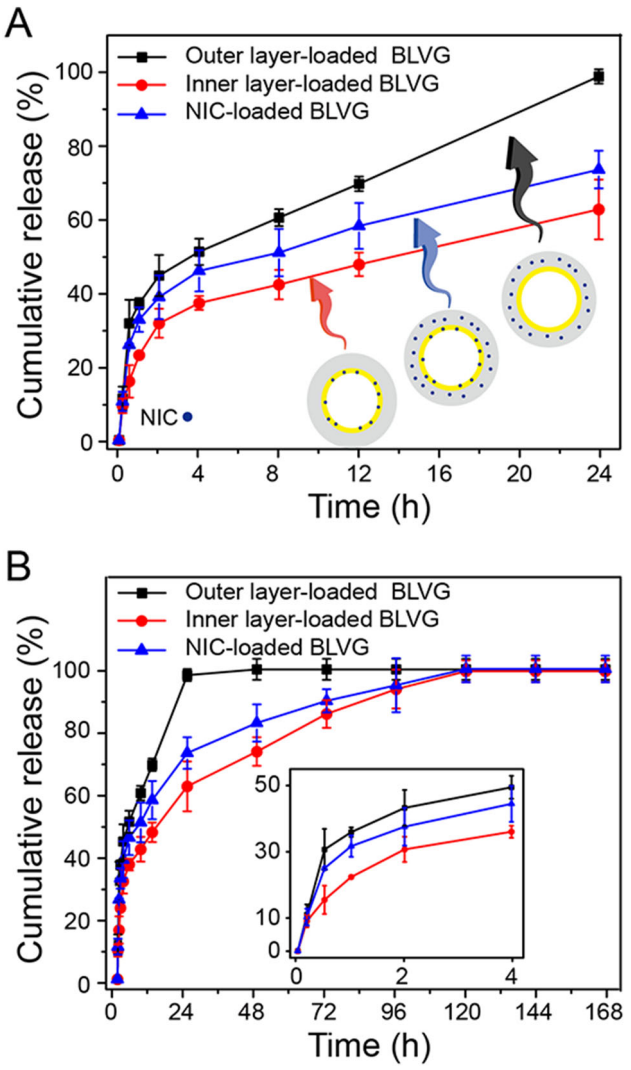

Fig. 6 In vitro release of NIC from different BLVG. **a** 24 h release of NIC. **b** 7 days release of NIC, the data points between 0 and 4 h was magnified and shown inside

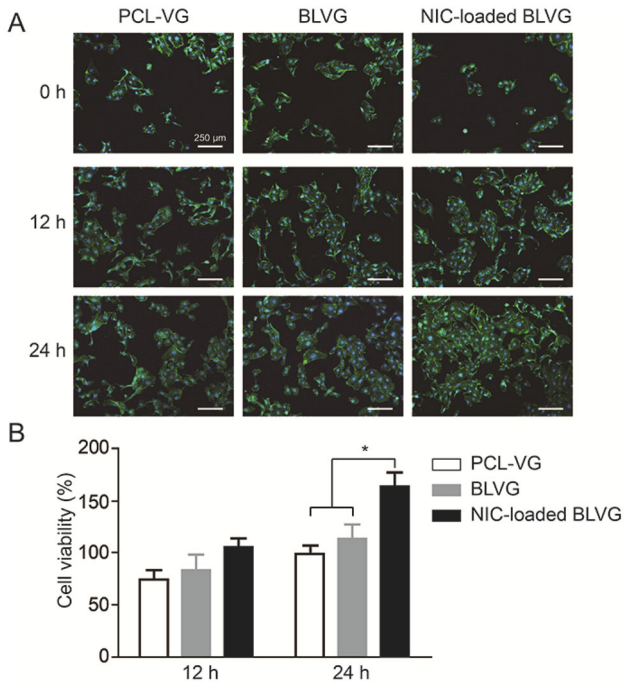

Fig. 7 Detection of proliferation capacity of ECs. **a** Fluorescent staining of ECs. **b** CCK-8 assay measuring the cell viability of ECs. $*p < 0.05$

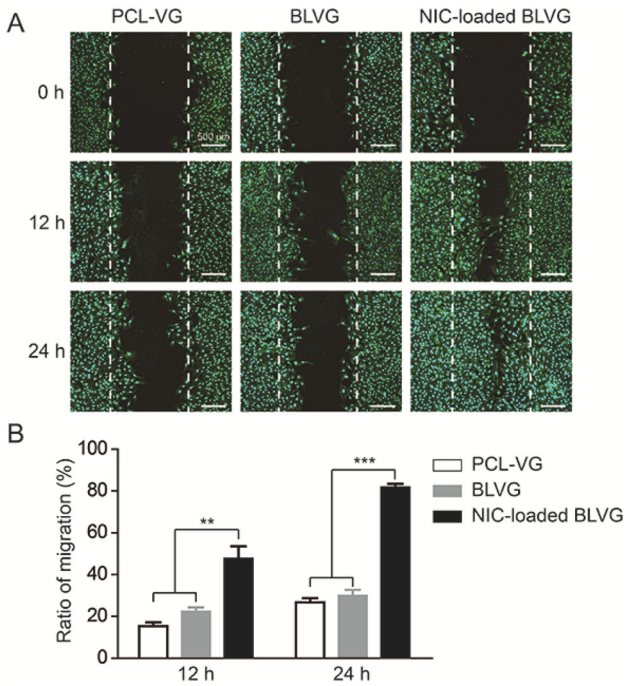

Fig. 8 Migration capacity of ECs. **a** Fluorescent staining after the wound healing assay of ECs. **b** Ratio of migration after culture ECs on different vascular grafts. $**p < 0.01$, $***p < 0.001$

capable of delivering drug rapidly after bypass surgery in the first 24 h and steadily releasing drug for over 4 days to continuously exert its biological activity. Thus, NIC-loaded BLVG could provide rapid onset and long-lasting regulation strategies on target cells, where the outer layer provided the rapid release and the inner layer provided the sustained release [47, 48]. Although the in vitro release study is under sink conditions, in vivo release process from NIC-loaded BLVG will provide valuable complimentary information.

NIC-loaded BLVG improved the proliferation capacity of ECs

ECs, living on the inner wall of human blood vessels, are a natural barrier to prevent thrombosis and anastomotic intimal hyperplasia [49]. Thus, enhancing EC function and facilitating spontaneous endothelialization are crucial for improving long-lasting patency rate of vascular grafts. Many efforts have been made in the field of developing novel vascular grafts with the ability of enhancing EC functions [50, 51].

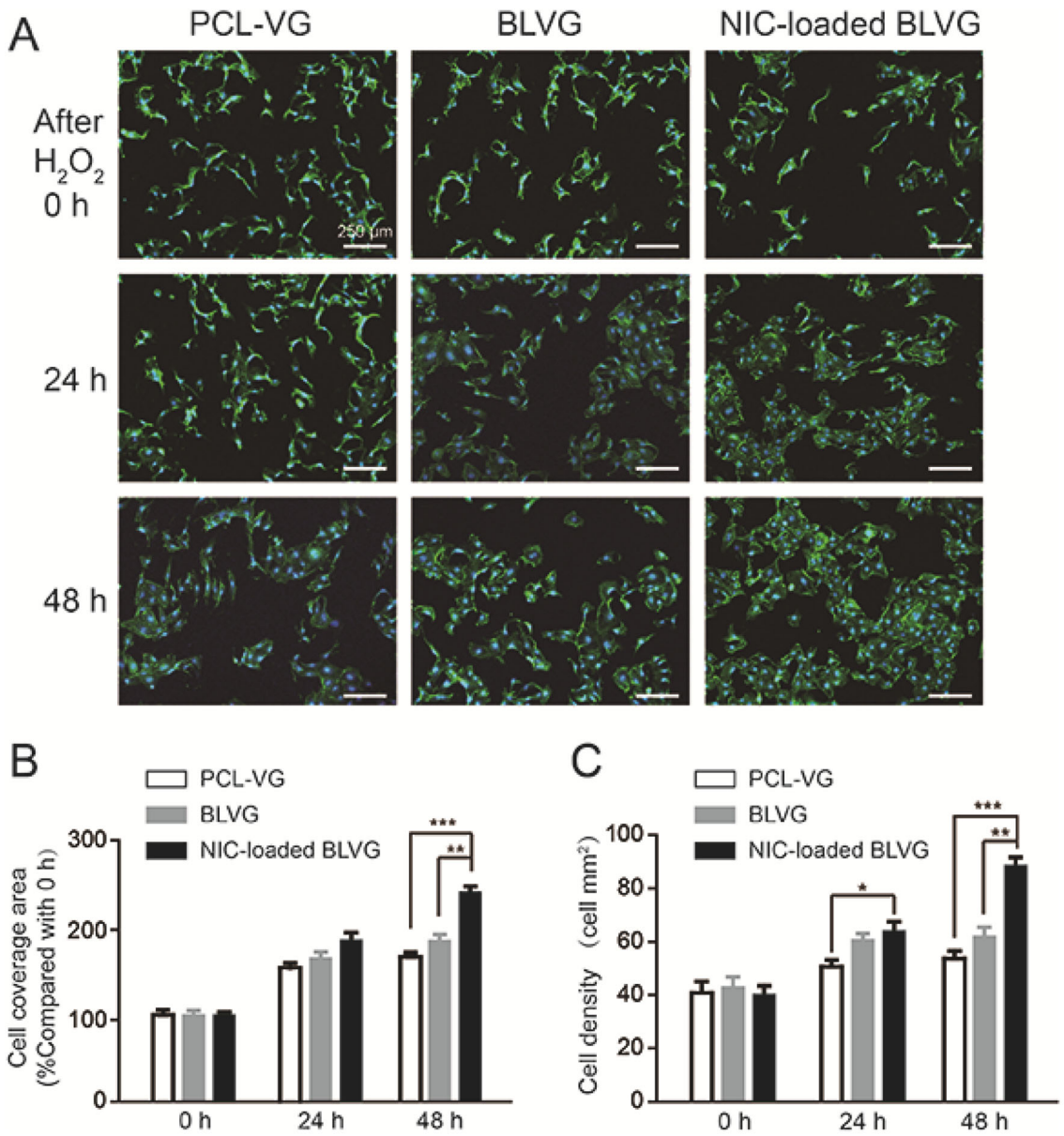

Fig. 9 Evaluation of antioxidation capacity of NIC-loaded BLVG. **a** Phalloidin/DAPI staining of ECs after H_2O_2 jury. **b** Relative cell coverage area of Phalloidin/DAPI staining images. **c** Cell density of ECs on different vascular grafts. *$p < 0.05$, **$p < 0.01$, ***$p < 0.001$

Our previous research showed that sulfated SF with outstanding biocompatibility and hemocompatibility was a suitable biomaterial for preparing vascular grafts. In addition, PCL, approved by FDA, was always used as the substrate of vascular graft to provide necessary mechanical properties [36].

To investigate the effect of vascular graft on cell proliferation, ECs were seeded onto 24-well plates and cultured for 12 h and 24 h, respectively. Figure 7a shows the fluorescence images of cytoskeleton and nucleus of ECs grown on different vascular grafts. It could be found that there was little difference in the proliferation of ECs on the three groups after culture for 12 h. However, the cell numbers of ECs became apparently different among PCL-VG, BLVG and NIC-loaded BLVG groups with the extension of culture time. Compared with PCL-VG and BLVG groups, the EC numbers of NIC-loaded BLVG group were significantly increased after 24 h of culture, indicating that the NIC released by NIC-loaded BLVG exerted its biological function to facilitate EC proliferation.

Cell viability was evaluated further using CCK-8 assay (Fig. 7b). The cell viabilities of BLVG and NIC-loaded BLVG groups were normalized as the relative percentage with respect to the PCL-VG group at 24 h which was specified as 100%. Compared with PCL-VG group and BLVG

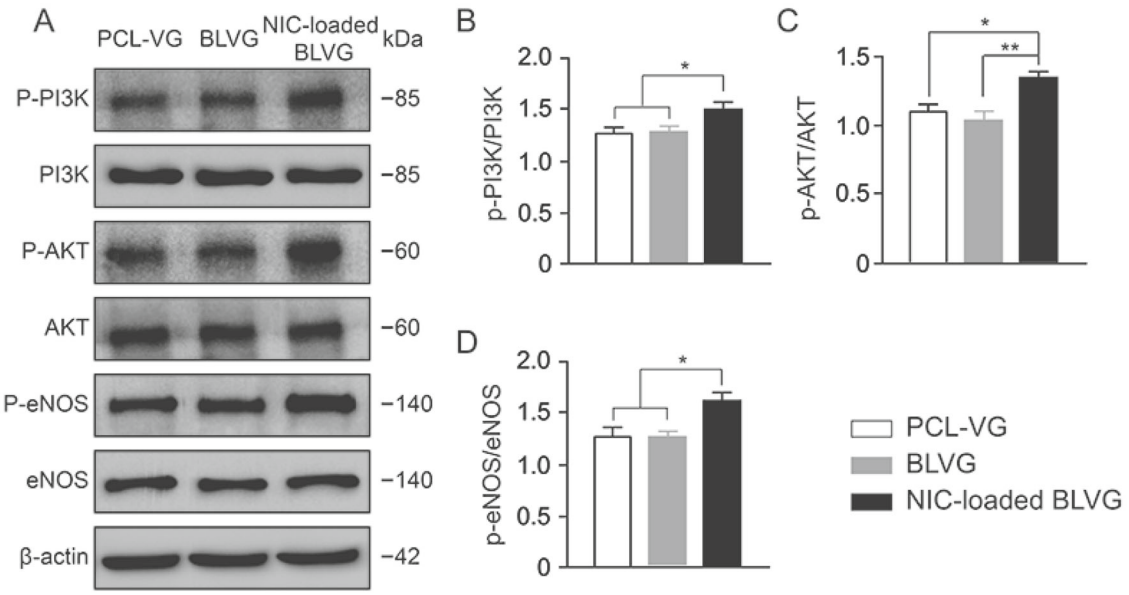

Fig. 10 NIC-loaded BLVG mediated the activation of PI3K/AKT/eNOS pathway. **a** Protein expression level of ECs including P-PI3K, PI3K, P-AKT, AKT, P-eNOS and eNOS. β-actin as the reference protein of samples. **b–d** Quantification of the western blot proteins in the ECs. *$p < 0.05$, **$p < 0.01$

groups, the cell viability of NIC-loaded BLVG group was increased after 12 h, but there were no statistically significant differences. After 48 h, the cell viability of NIC-loaded BLVG was significantly increased than the other two groups. The results of EC staining and CCK-8 assay demonstrated that NIC-loaded BLVG had a great potential in improving the proliferation ability of ECs.

NIC-loaded BLVG improved the migration capacity of ECs

The ability of EC migration is critical during the endothelialization of vascular grafts after implantation [52]. The patients who require bypass surgery often combine with other chronic diseases. ECs of these patients are usually affected by oxidative stress, inflammatory response and other factors, which lead to the reduce of EC functions including migration capacity, etc. [53]. Therefore, vascular grafts which have the capability of improving EC migration ability will be more conducive to rapid endothelialization in vivo and meeting the clinical needs.

The wound healing assay was used to evaluate the migration ability of ECs cultured on different vascular grafts. As shown in Fig. 8a, the distance between wounds in each group was equal at 0 h. After 12 h of culture, the migration ratio of ECs on NIC-loaded BLVG significantly increased and reached $47.6 \pm 5.9\%$. After 24 h of culture, the wound in NIC-loaded BLVG group nearly disappeared with the migration ratio reaching $81.7 \pm 1.7\%$. The migration ratio of ECs on BLVG group increased slightly compared with PCL-VG group, suggesting the great cytocompatibility of the sulfated SF layer. The statistical graph of the migration ratio is shown in Fig. 8b. Hence, we speculated that NIC could not only improve the proliferation ability of ECs, but also facilitate EC migration. But the biological mechanism behind still needs future study.

NIC-loaded BLVG increased the antioxidation capacity of ECs

Many researches indicated that NIC could restore endothelial dysfunction caused by some chronic diseases through its antioxidative effects [54]. Therefore, a H_2O_2-induced EC oxidative injury model was used to validate the effects of NIC-loaded BLVG. As shown in Fig. 9a, cell morphology was evaluated by using phalloidin/DAPI staining after ECs damaged by H_2O_2. The cell morphology of 0 h after H_2O_2 injury groups appeared significant changes including cell shrinkage, twisting and clustering, which was the most common characteristic eluding to damage [55]. However, after culture on different vascular grafts for 24 h, compared with PCL-VG group, the cell numbers of NIC-loaded BLVG group significantly increased, and the cell morphology also gradually became round shape as a recovering feature. After 48 h of culture, the cell density of NIC-loaded BLVG group significantly increased than the other two groups (Fig. 9b and c). Culturing ECs with NIC-loaded BLVG also exhibited better cellular morphology restoration after 48 h. There were still many shrunk and twisted ECs in PCL-VG and BLVG groups, indicating that the ECs damaged by H_2O_2 did not

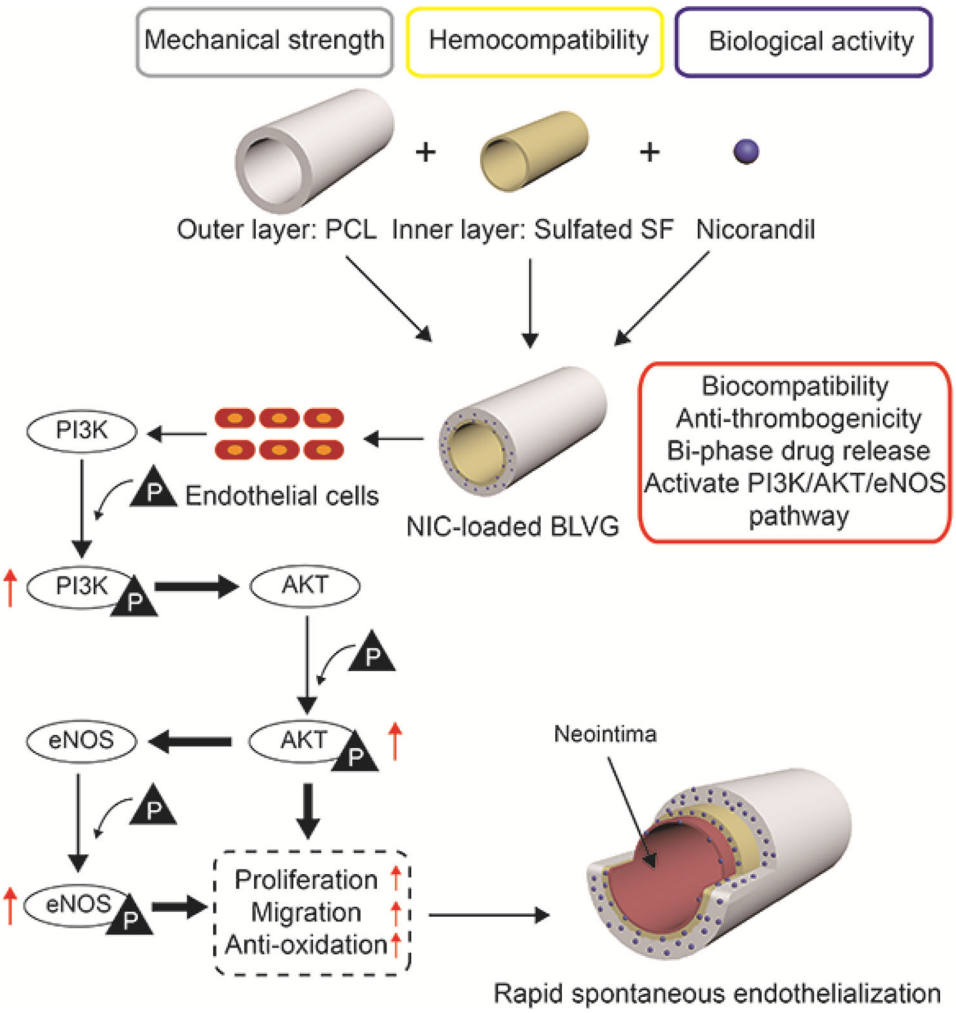

Fig. 11 Schematic diagram of the biological functions of NIC-loaded BLVG

recover even after 2 days. Thus, we speculated that the cell functions of these ECs including proliferation and migration capacity were lower than healthy ECs, just like the ECs living in the vascular system of patients with chronic diseases. This result further illustrated the importance of adding NIC as a bioactive substance in BLVG. The effect of NIC-loaded BLVG against cellular oxidative injury was most likely to be related to NIC scavenging ability of intracellular reactive oxygen species (ROS). Cellular oxidative damage is a well-established mechanism leading to the cell injury. ROS binds with most normal cellular components, reacting with unsaturated bonds of membrane lipid, denaturing proteins and attacking nucleic acids [56].

NIC-loaded BLVG activates PI3K/AKT/eNOS signaling pathway of ECs

The PI3K/AKT/eNOS signaling pathway is widely involved in crucial physiological processes such as cell energy metabolism, oxidative stress and cell proliferation, which plays an important role in cell damage caused by various diseases [57, 58]. NIC, as a KATP channel opener combined with NO donor activity and antioxidant activity, has been reported to improve endothelial colony-forming cell (ECFC) functions through activating AKT/eNOS signaling [59]. In addition, NIC could also alleviate the apoptosis of cardiomyocytes via PI3K/AKT signaling [60]. Thus, we speculated that the biological activity of NIC on EC function could be related to the PI3K/AKT/eNOS pathway.

To determine the possible molecular mechanism, western blot assay was used to analyze the protein expression of ECs after being cultured on different vascular grafts. As shown in Fig. 10, the expression levels of PI3K, AKT and eNOS were not significantly changed after being cultured for 24 h. However, the phosphorylation levels of PI3K, AKT and eNOS were significantly increased, suggesting the enhancement effects of NIC on the phosphorylation levels, thereby improving the proliferation, migration function and antioxidant capacity of ECs. Moreover, it was reported that NIC

could activate PI3K/AKT pathway to improve cell functions and play a protective role in vivo [60].

The biological functions of NIC have also been reported by activating MAPK, NF-κb, even JAK/STAT signaling pathways [61, 62]. The summary diagram including the structure of NIC-loaded BLVG, in vitro cell study part and the possible molecular mechanism of this study is shown in Fig. 11. But in-depth study of biological mechanisms still need further research in vivo. Understanding the biological mechanism will provide a better foundation of subsequent clinical application and also provide novel ideas for other researchers to develop advanced vascular graft.

Conclusions

In summary, NIC-loaded BLVG was fabricated by PCL and sulfated SF using electrospinning technology. The fabrication procedure homogeneously blended the bioactive components (NIC) in both outer and inner layers of the vascular graft, endowing NIC-loaded BLVG a biphasic release behavior. In vitro study showed that NIC-loaded BLVG significantly increased the proliferative, migration and antioxidant capacity of ECs, which might help NIC-loaded BLVG to complete rapid spontaneous endothelialization after bypass surgery. In addition, we also tried to confirm the biological mechanism behind these functions of NIC-loaded BLVG. It was found that NIC-loaded BLVG could significantly activate the PI3K/AKT/eNOS pathway in ECs. Therefore, this study suggested that NIC-loaded BLVG was a safe and efficacious vascular graft, which provided a new idea for the clinical translational potential of small-diameter vascular graft.

Acknowledgements This work was supported by the National Natural Science Foundation of China (31771058, 32071359, 11421202, 61227902 and 11120101001), National Key Technology R&D Program (2016YFC1100704, 2016YFC1101101), International Joint Research Center of Aerospace Biotechnology and Medical Engineering from Ministry of Science and Technology of China, 111 Project (B13003), Research Fund for the Doctoral Program of Higher Education of China (20131102130004) and Fundamental Research Funds for the Central Universities.

Author contributions ZX and HFL took part in conceptualization; ZX, CCZ and HFL contributed to methodology; ZX and CZ carried out investigation; ZX wrote the original draft; all authors wrote, reviewed and edited the final manuscirpt; HFL acquired funding; YBF and HFL contributed to resources; and HFL conducted supervision.

Compliance with ethical standards

Conflict of interest Zheng Xing, Chen Zhao, Chunchen Zhang, Yubo Fan and Haifeng Liu declare that they have no conflict of interest.

Ethical approval All the procedures followed were in accordance with the ethical standards of the responsible committee on human experimentation (institutional and national) and with the Helsinki Declaration of 1975, as revised in 2008 (5). Informed consent was obtained from all patients for being included in the study.

References

1. Ehrmann K, Potzmann P, Dworak C, Bergmeister H, Eilenberg M, Grasl C, Koch T, Schima H, Liska R, Baudis S (2020) Hard block degradable polycarbonate urethanes: promising biomaterials for electrospun vascular prostheses. Biomacromol 21(2):376–387. https://doi.org/10.1021/acs.biomac.9b01255
2. Mathers CD, Loncar D (2006) Projections of global mortality and burden of disease from 2002 to 2030. PLoS Med 3(11):e442. https://doi.org/10.1371/journal.pmed.0030442
3. Bangalore S, Guo Y, Samadashvili Z, Blecker S, Xu J, Hannan EL (2015) Everolimus-eluting stents or bypass surgery for multivessel coronary disease. New Engl J Med 372(13):1213–1222. https://doi.org/10.1161/CIRCINTERVENTIONS.115.002626
4. Wang Z, Mithieux SM, Weiss AS (2019) Fabrication techniques for vascular and vascularized tissue engineering. Adv Healthc Mater 8(19):1900742. https://doi.org/10.1002/adhm.201900742
5. Wang Y, Ma B, Yin A, Zhang B, Luo R, Pan J, Wang Y (2020) Polycaprolactone vascular graft with epigallocatechin gallate embedded sandwiched layer-by-layer functionalization for enhanced antithrombogenicity and anti-inflammation. J Control Release 320:226–238. https://doi.org/10.1016/j.jconrel.2020.01.043
6. Jin X, Geng X, Jia L, Xu Z, Ye L, Gu Y, Zhang AY, Feng ZG (2019) Preparation of small-diameter tissue-engineered vascular grafts electrospun from heparin end-capped PCL and evaluation in a rabbit carotid artery replacement model. Macromol Biosci 19(8):1900114. https://doi.org/10.1002/mabi.201900114
7. Gimbrone Michael A, García-Cardeña G (2016) Endothelial cell dysfunction and the pathobiology of atherosclerosis. Circ Res 118(4):620–636. https://doi.org/10.1161/CIRCRESAHA.115.306301
8. Xie RY, Fang XL, Zheng XB, Lv WZ, Li YJ, Ibrahim Rage H, He QL, Zhu WP, Cui TX (2019) Salidroside and FG-4592 ameliorate high glucose-induced glomerular endothelial cells injury via HIF upregulation. Biomed Pharmacother 118:109175. https://doi.org/10.1016/j.biopha.2019.109175
9. Zhang J, Shi J, Ma H, Liu L, He L, Qin C, Zhang D, Guo Y, Gong R (2020) The placental growth factor attenuates intimal hyperplasia in vein grafts by improving endothelial dysfunction. Eur J Pharmacol 868:172856. https://doi.org/10.1016/j.ejphar.2019.172856
10. Chen CC, Hong HJ, Hao WR, Cheng TH, Liu JC, Sung LC (2019) Nicorandil prevents doxorubicin-induced human umbilical vein endothelial cell apoptosis. Eur J Pharmacol 859:172542. https://doi.org/10.1016/j.ejphar.2019.172542
11. Umaru B, Pyriochou A, Kotsikoris V, Papapetropoulos A, Topouzis S (2015) ATP-sensitive potassium channel activation induces angiogenesis in vitro and in vivo. J Pharmacol Exp Ther 354(1):79–87. https://doi.org/10.1124/jpet.114.222000
12. Serizawa K-i, Yogo K, Aizawa K, Tashiro Y, Ishizuka N (2011) Nicorandil prevents endothelial dysfunction due to antioxidative effects via normalisation of NADPH oxidase and nitric oxide synthase in streptozotocin diabetic rats. Cardiovasc Diabetol 10(1):105. https://doi.org/10.1186/1475-2840-10-105
13. Horinaka S, Kobayashi N, Yagi H, Mori Y, Matsuoka H (2006) Nicorandil but not ISDN upregulates endothelial nitric oxide synthase expression, preventing left ventricular remodeling and degradation of cardiac function in dahl salt-sensitive hyperten-

sive rats with congestive heart failure. J Cardiovasc Pharmacol 47(5):629–635. https://doi.org/10.1097/01.fjc.0000211741.47960.c2
14. Joo Myung L, Daiki K, Maki O, Mamoru T, Hiroaki T, Katsuhisa W, Tetsuya A, Akiyoshi K, Hiroki I, Woo-Hyun L, Joon-Hyung D, Chang-Wook N, Nobuhiro T, Bon-Kwon K, Nobukiyo T (2016) Safety and efficacy of intracoronary nicorandil as hyperaemic agent for invasive physiological assessment: a patient-level pooled analysis. EuroIntervention 12(2):208–215. https://doi.org/10.4244/EIJV12I2A34
15. Mao D, Zhu M, Zhang X, Ma R, Yang X, Ke T, Wang L, Li Z, Kong D, Li C (2017) A macroporous heparin-releasing silk fibroin scaffold improves islet transplantation outcome by promoting islet revascularisation and survival. Acta Biomater 59:210–220. https://doi.org/10.1016/j.actbio.2017.06.039
16. Raia NR, Jia D, Ghezzi CE, Muthukumar M, Kaplan DL (2020) Characterization of silk-hyaluronic acid composite hydrogels towards vitreous humor substitutes. Biomaterials 233:119729. https://doi.org/10.1016/j.biomaterials.2019.119729
17. Tozzi L, Laurent PA, Di Buduo CA, Mu X, Massaro A, Bretherton R, Stoppel W, Kaplan DL, Balduini A (2018) Multi-channel silk sponge mimicking bone marrow vascular niche for platelet production. Biomaterials 178:122–133. https://doi.org/10.1016/j.biomaterials.2018.06.018
18. Rodriguez M, Kluge JA, Smoot D, Kluge MA, Schmidt DF, Paetsch CR, Kim PS, Kaplan DL (2020) Fabricating mechanically improved silk-based vascular grafts by solution control of the gel-spinning process. Biomaterials 230:119567. https://doi.org/10.1016/j.biomaterials.2019.119567
19. Gupta P, Lorentz KL, Haskett DG, Cunnane EM, Ramaswamy AK, Weinbaum JS, Vorp DA, Mandal BB (2020) Bioresorbable silk grafts for small diameter vascular tissue engineering applications: in vitro and in vivo functional analysis. Acta Biomater 105:146–158. https://doi.org/10.1016/j.actbio.2020.01.020
20. Li H, Wang Y, Sun X, Tian W, Xu J, Wang J (2019) Steady-state behavior and endothelialization of a silk-based small-caliber scaffold in vivo transplantation. Polymers (Basel) 11(8):1303. https://doi.org/10.3390/polym11081303
21. Liu H, Li X, Zhou G, Fan H, Fan Y (2011) Electrospun sulfated silk fibroin nanofibrous scaffolds for vascular tissue engineering. Biomaterials 32(15):3784–3793. https://doi.org/10.1016/j.biomaterials.2011.02.002
22. Liu H, Li X, Niu X, Zhou G, Li P, Fan Y (2011) Improved hemocompatibility and endothelialization of vascular grafts by covalent immobilization of sulfated silk fibroin on poly(lactic-co-glycolic acid) scaffolds. Biomacromol 12(8):2914–2924. https://doi.org/10.1021/bm200479f
23. Gong X, Liu H, Ding X, Liu M, Li X, Zheng L, Jia X, Zhou G, Zou Y, Li J, Huang X, Fan Y (2014) Physiological pulsatile flow culture conditions to generate functional endothelium on a sulfated silk fibroin nanofibrous scaffold. Biomaterials 35(17):4782–4791. https://doi.org/10.1016/j.biomaterials.2014.02.050
24. Wu T, Zhang J, Wang Y, Li D, Sun B, El-Hamshary H, Yin M, Mo X (2018) Fabrication and preliminary study of a biomimetic tri-layer tubular graft based on fibers and fiber yarns for vascular tissue engineering. Mater Sci Eng C Mater Biol Appl 82:121–129. https://doi.org/10.1016/j.msec.2017.08.072
25. Yin A, Zhuang W, Liu G, Lan X, Tang Z, Deng Y, Wang Y (2020) Performance of PEGylated chitosan and poly (L-lactic acid-co-ε-caprolactone) bilayer vascular grafts in a canine femoral artery model. Colloids Surf B 188:110806. https://doi.org/10.1016/j.colsurfb.2020.110806
26. Yan S, Napiwocki B, Xu Y, Zhang J, Zhang X, Wang X, Crone WC, Li Q, Turng L-S (2020) Wavy small-diameter vascular graft made of eggshell membrane and thermoplastic polyurethane. Mater Sci Eng C Mater Biol Appl 107:110311. https://doi.org/10.1016/j.msec.2019.110311
27. Du H, Tao L, Wang W, Liu D, Zhang Q, Sun P, Yang S, He C (2019) Enhanced biocompatibility of poly(l-lactide-co-epsilon-caprolactone) electrospun vascular grafts via self-assembly modification. Mater Sci Eng C Mater Biol Appl 100:845–854. https://doi.org/10.1016/j.msec.2019.03.063
28. Norouzi SK, Shamloo A (2019) Bilayered heparinized vascular graft fabricated by combining electrospinning and freeze drying methods. Mater Sci Eng C Mater Biol Appl 94:1067–1076. https://doi.org/10.1016/j.msec.2018.10.016
29. Gong W, Lei D, Li S, Huang P, Qi Q, Sun Y, Zhang Y, Wang Z, You Z, Ye X, Zhao Q (2016) Hybrid small-diameter vascular grafts: Anti-expansion effect of electrospun poly ε-caprolactone on heparin-coated decellularized matrices. Biomaterials 76:359–370. https://doi.org/10.1016/j.biomaterials.2015.10.066
30. Seyed S, Zargarian V, Haddadi-Asl Z, Kafrashian M, Azarnia M (2018) Surfactant-assisted-water-exposed versus surfactant-aqueous-solution-exposed electrospinning of novel super hydrophilic polycaprolactone based fibers: analysis of drug release behavior. J Biomed Mater Res Part A 8:675–682. https://doi.org/10.1002/jbm.a.36575
31. Barbara V, Silvia R, Giuseppina S, Maria C, Bonferoni G (2018) Coated electrospun alginate-containing fibers as novel delivery systems for regenerative purposes. Int J Nanomed 10:17–25. https://doi.org/10.2147/IJN.S175069
32. Yang Y, Lei D, Zou H, Huang S, Yang Q, Li S, Qing FL, Ye X, You Z, Zhao Q (2019) Hybrid electrospun rapamycin-loaded small-diameter decellularized vascular grafts effectively inhibit intimal hyperplasia. Acta Biomater 97:321–332. https://doi.org/10.1016/j.actbio.2019.06.037
33. Shi J, Zhang X, Jiang L, Zhang L, Dong Y, Midgley AC, Kong D, Wang S (2019) Regulation of the inflammatory response by vascular grafts modified with Aspirin-Triggered Resolvin D1 promotes blood vessel regeneration. Acta Biomater 97:360–373. https://doi.org/10.1016/j.actbio.2019.07.037
34. Xing Z, Zhang C, Zhao C, Ahmad Z, Li JS, Chang MW (2018) Targeting oxidative stress using tri-needle electrospray engineered Ganoderma lucidum polysaccharide-loaded porous yolk-shell particles. Eur J Pharm Sci 125:64–73. https://doi.org/10.1016/j.ejps.2018.09.016
35. Yao D, Peng G, Qian Z, Niu Y, Liu H, Fan Y (2017) Regulating coupling efficiency of REDV by controlling silk fibroin structure for vascularization. ACS Biomater Sci Eng 3:489–501. https://doi.org/10.1021/acsbiomaterials.7b00553
36. Wang Z, Cui Y, Wang J, Yang X, Wu Y, Wang K, Gao X, Li D, Li Y, Zheng X-L, Zhu Y, Kong D, Zhao Q (2014) The effect of thick fibers and large pores of electrospun poly(ε-caprolactone) vascular grafts on macrophage polarization and arterial regeneration. Biomaterials 35(22):5700–5710. https://doi.org/10.1016/j.biomaterials.2014.03.078
37. Chatterjee S, Judeh ZMA (2015) Encapsulation of fish oil with N-stearoyl O-butylglyceryl chitosan using membrane and ultrasonic emulsification processes. Carbohydr Polym 123:432–442. https://doi.org/10.1016/j.carbpol.2015.01.072
38. Moomand K, Lim LT (2014) Oxidative stability of encapsulated fish oil in electrospun zein fibres. Food Res Int 62:523–532. https://doi.org/10.1016/j.foodres.2014.03.054
39. Singh B, Garg T, Goyal AK, Rath G (2016) Development, optimization, and characterization of polymeric electrospun nanofiber: a new attempt in sublingual delivery of nicorandil for the management of angina pectoris. Artif Cells Nanomed Biotechnol 44(6):1498–1507. https://doi.org/10.3109/21691401.2015.1052472
40. Yao D, Qian Z, Zhou J, Peng G, Zhou G, Liu H, Fan Y (2018) Facile incorporation of REDV into porous silk fibroin scaffolds for

enhancing vascularization of thick tissues. Mater Sci Eng C Mater Biol Appl 93:96–105. https://doi.org/10.1016/j.msec.2018.07.062
41. Wei Y, Wu Y, Zhao R, Zhang K, Midgley AC, Kong D, Li Z, Zhao Q (2019) MSC-derived sEVs enhance patency and inhibit calcification of synthetic vascular grafts by immunomodulation in a rat model of hyperlipidemia. Biomaterials 204:13–24. https://doi.org/10.1016/j.biomaterials.2019.01.049
42. Liu Y, Xue X, Zhang H, Che X, Luo J, Wang P, Xu J, Xing Z, Yuan L, Liu Y, Fu X, Su D, Sun S, Zhang H, Wu C, Yang J (2019) Neuronal-targeted TFEB rescues dysfunction of the autophagy-lysosomal pathway and alleviates ischemic injury in permanent cerebral ischemia. Autophagy 15(3):493–509. https://doi.org/10.1080/15548627.2018.1531196
43. Wang M, Wang Y, Chen Y, Gu H (2013) Improving endothelialization on 316L stainless steel through wettability controllable coating by sol–gel technology. Appl Surf Sci 268:73–78. https://doi.org/10.1016/j.apsusc.2012.11.159
44. Lee JH, Lee SJ, Khang G, Lee HB (2000) The effect of fluid shear stress on endothelial cell adhesiveness to polymer surfaces with wettability gradient. J Colloid Interface Sci 230(1):84–90. https://doi.org/10.1006/jcis.2000.7080
45. Shi J, Chen S, Wang L, Zhang X, Gao J, Jiang L, Tang D, Zhang L, Midgley A, Kong D, Wang S (2019) Rapid endothelialization and controlled smooth muscle regeneration by electrospun heparin-loaded polycaprolactone/gelatin hybrid vascular grafts. J Biomed Mater Res Part B 107(6):2040–2049. https://doi.org/10.1002/jbm.b.34295
46. Tseders ÉÉ, Purinya BA (1975) The mechanical properties of human blood vessels relative to their location. Polym Mech 11(2):271–275. https://doi.org/10.1007/BF00854734
47. Ye P, Wei S, Luo C, Wang Q, Li A, Wei F (2020) Long-term effect against methicillin-resistant staphylococcus aureus of emodin released from coaxial electrospinning nanofiber membranes with a biphasic profile. Biomolecules 10(3):362. https://doi.org/10.3390/biom10030362
48. Tort S, Han D, Steckl AJ (2020) Self-inflating floating nanofiber membranes for controlled drug delivery. Int J Pharm 579:119164. https://doi.org/10.1016/j.ijpharm.2020.119164
49. Qu B, Yuan L, Yang L, Li J, Lv H, Yang X (2019) Polyurethane end-capped by tetramethylpyrazine-nitrone for promoting endothelialization under oxidative stress. Adv Healthc Mater 8(20):1900582. https://doi.org/10.1002/adhm.201900582
50. Wang Z, Lu Y, Qin K, Wu Y, Tian Y, Wang J, Zhang J, Hou J, Cui Y, Wang K, Shen J, Xu Q, Kong D, Zhao Q (2015) Enzyme-functionalized vascular grafts catalyze in-situ release of nitric oxide from exogenous NO prodrug. J Control Release 210:179–188. https://doi.org/10.1016/j.jconrel.2015.05.283
51. Yang J, Wei K, Wang Y, Li Y, Ding N, Huo D, Wang T, Yang G, Yang M, Ju T, Zeng W, Zhu C (2018) Construction of a small-caliber tissue-engineered blood vessel using icariin-loaded β-cyclodextrin sulfate for in situ anticoagulation and endothelialization. Sci China Life Sci 61(10):1178–1188. https://doi.org/10.1007/s11427-018-9348-9
52. Guo X, Wang X, Li X, Jiang YC, Han S, Ma L, Guo H, Wang Z, Li Q (2020) Endothelial cell migration on poly(ε-caprolactone) nanofibers coated with a nanohybrid Shish–Kebab structure mimicking collagen fibrils. Biomacromol 21(3):1202–1213. https://doi.org/10.1021/acs.biomac.9b01638
53. Wang Z, Zheng W, Wu Y, Wang J, Zhang X, Wang K, Zhao Q, Kong D, Ke T, Li C (2016) Differences in the performance of PCL-based vascular grafts as abdominal aorta substitutes in healthy and diabetic rats. Biomater Sci 4(10):1485–1492. https://doi.org/10.1039/C6BM00178E
54. Xu X, Liu X, Yu L, Ma J, Yu S, Ni M (2020) Impact of intracoronary nicorandil before stent deployment in patients with acute coronary syndrome undergoing percutaneous coronary intervention. Exp Ther Med 19(1):137–146. https://doi.org/10.3892/etm.2019.8219
55. Yang HL, Korivi M, Chen CH, Peng WJ, Chen CS, Li ML, Hsu LS, Liao JW, Hseu YC (2017) Antrodia camphorata attenuates cigarette smoke-induced ROS production, DNA damage, apoptosis, and inflammation in vascular smooth muscle cells, and atherosclerosis in ApoE-deficient mice. Environ Toxicol 32(8):2070–2084. https://doi.org/10.1002/tox.22422
56. Fojta M, Daňhel A, Havran L, Vyskočil V (2016) Recent progress in electrochemical sensors and assays for DNA damage and repair. TrAC Trends Anal Chem 79(5):160–167. https://doi.org/10.1016/j.trac.2015.11.018
57. Carrizzo A, Conte Giulio M, Sommella E, Damato A, Ambrosio M, Sala M, Scala Maria C, Aquino Rita P, De Lucia M, Madonna M, Sansone F, Ostacolo C, Capunzo M, Migliarino S, Sciarretta S, Frati G, Campiglia P, Vecchione C (2019) Novel potent decameric peptide of spirulina platensis reduces blood pressure levels through a PI3K/AKT/eNOS-dependent mechanism. Hypertension 73(2):449–457. https://doi.org/10.1161/HYPERTENSIONAHA.118.11801
58. Ahmad KA, Ze H, Chen J, Khan FU, Xuezhuo C, Xu J, Qilong D (2018) The protective effects of a novel synthetic β-elemene derivative on human umbilical vein endothelial cells against oxidative stress-induced injury: involvement of antioxidation and PI3k/Akt/eNOS/NO signaling pathways. Biomed Pharmacother 106:1734–1741. https://doi.org/10.1016/j.biopha.2018.07.107
59. Wu Y, He MY, Ye JK, Ma SY, Huang W, Wei YY, Kong H, Wang H, Zeng XN, Xie WP (2017) Activation of ATP-sensitive potassium channels facilitates the function of human endothelial colony-forming cells via Ca2+/Akt/eNOS pathway. J Cell Mol Med 21(3):609–620. https://doi.org/10.1111/jcmm.13006
60. Wang X, Pan J, Liu D, Zhang M, Li X, Tian J, Liu M, Jin T, An F (2019) Nicorandil alleviates apoptosis in diabetic cardiomyopathy through PI3K/Akt pathway. J Cell Mol Med 23(8):5349–5359. https://doi.org/10.1111/jcmm.14413
61. Huang WC, Lai CL, Liang YT, Hung HC, Liou CJ (2016) Phloretin attenuates LPS-induced acute lung injury in mice via modulation of the NF-κB and MAPK pathways. Int Immunopharmacol 40:98–105. https://doi.org/10.1016/j.intimp.2016.08.035
62. Gaafar AGA, Messiha BAS, Abdelkafy AML (2018) Nicorandil and theophylline can protect experimental rats against complete Freund's adjuvant-induced rheumatoid arthritis through modulation of JAK/STAT/RANKL signaling pathway. Eur J Pharmacol 822:177–185. https://doi.org/10.1016/j.ejphar.2018.01.009